ROYAL SOCIETY
OF CHEMISTRY

EDGE ARTICLE

Check for updates

Pb₂(SeO₃)(SiF₆): the first selenite fluorosilicate with a wide bandgap and large birefringence achieved through perfluorinated group modification†

Peng-Fei Li, [ID] [ab] Chun-Li Hu,[ab] Jiang-Gao Mao [ID] [ab] and Fang Kong [ID] *[ab]

Birefringent crystals serve as the core elements of polarizing optical devices. However, the inherent challenge of balancing bandgap and birefringence poses a significant hurdle in designing crystals with excellent overall performance. In this study, we propose a novel approach, namely modification with perfluorinated groups, to achieve dual enhancement of the bandgap and birefringence of selenite materials. We have successfully synthesized the first selenite fluorosilicate, namely, Pb₂(SeO₃)(SiF₆). This compound exhibits a three-dimensional structure composed of two-dimensional lead selenite layers bridged by SiF₆ octahedrons. Notably, by introducing a perfluorinated SiF₆ group, the bandgap of the lead selenite compound has been expanded to 4.4 eV. Furthermore, Pb₂(SeO₃)(SiF₆) demonstrates a large birefringence (0.161 @ 546 nm), surpassing most of the selenite compounds with a bandgap larger than 4.2 eV. Theoretical calculations suggest that the large birefringence of Pb₂(SeO₃)(SiF₆) can be attributed to the synergistic effects of SeO₃, PbO₄ and PbO₃F₄ polyhedrons. Our research not only pioneers a new system for selenite materials, enriching the diversity of selenite structures, but also provides a design methodology for obtaining wide bandgap birefringent selenite.

Introduction

Birefringent crystals play a pivotal role as optical functional components in commercial, agricultural, industrial, and military sectors.[1–4] Some crystals have been commercialized, such as α-BaB₂O₄,[5] CaCO₃,[6] YVO₄,[7] MgF₂,[8] TiO₂,[9] *etc.* However, these commercially available birefringent crystals have inherent limitations. For example, the transparency of YVO₄ is notably low below 400 nm, and the birefringence of MgF₂ is comparatively small, which fail to meet the demands of modern industry.[10] In recent years, with the rapid advancement of optoelectronic technology, the requirement for miniaturization of short-wave devices has been escalating. The miniaturization of such devices necessitates crystals with large birefringence and a wide bandgap.[11,12] However, the inherent contradiction between the bandgap and birefringence makes wide bandgap birefringent crystals extremely rare. Consequently, addressing these contradictions and achieving a balance between these

properties is an urgent issue that requires immediate attention.[13–17]

Metal selenites, containing stereo-chemically active lone pair electrons, have shown promise as potential candidates for birefringent materials due to their significant anisotropy.[18,19] Scientists have primarily explored the following avenues to enhance the birefringent performance of selenite crystals: (i) incorporation of stereo-chemically active lone pair cations, such as Pb₂Bi(SeO₃)₂Cl₃ (0.186 @ 1064 nm, 3.45 eV),[20] Rb₂Bi₂(-SeO₃)₃F₂ (0.105 @ 546 nm, 3.72 eV),[21] and Bi₄TeO₄F₂(TeO₃)(-SeO₃)₂ (0.20 @ 1064 nm, 2.74 eV);[22] (ii) incorporation of d⁰ transition metals susceptible to second-order Jahn–Teller (SOJT) distortion, for example, Pb₂(V₂O₄F)(VO₂)(SeO₃)₃ (0.105 @ 1064 nm, 2.35 eV),[23] Bi₄TiO₂F₄(SeO₃)₄ (0.19 @ 1064 nm, 3.58 eV)[22] and Gd₂F₂(OH₂)(MoO₃)₂(SeO₃)₂ (0.143 @ 1064 nm, 3.15 eV);[24] (iii) incorporation of highly polarizable and deformable d¹⁰ transition metals, for instance, Rb₂Hg₂(SeO₃)₃ (0.055 @ 546 nm, 3.60 eV),[25] Pb₂Cd(SeO₃)₂Cl₂ (0.093 @ 1064 nm, 4.1 eV)[26] and Pb₂Cd(SeO₃)₂Br₂ (0.116 @ 1064 nm, 3.9 eV).[26] However, the relatively low transparency below 400 nm limits their application in the ultraviolet region. To address this, researchers have introduced ions conducive to widening the bandgap in the selenite system, such as alkali metals, alkaline earth metals, *etc.*[27] The successfully synthesized wide bandgap selenites include NaLu(SeO₃)₂ (0.153 @ 546 nm, 5.3 eV),[28] Ga₂(SeO₃)₃(-H₂O)₃ (0.082 @ 532 nm, 5.3 eV),[29] and Y(HSeO₃)(SeO₃)(H₂-O)·(H₂O) (0.044 @ 532 nm, 5.5 eV).[30] Although their bandgaps have been improved to 5.0 eV or above, their birefringence

ᵃState Key Laboratory of Structural Chemistry, Fujian Institute of Research on the Structure of Matter, Chinese Academy of Sciences, Fuzhou 350002, P. R. China. E-mail: kongfang@fjirsm.ac.cn

ᵇUniversity of Chinese Academy of Sciences, Beijing 100049, P. R. China

decreased obviously, except for $NaLu(SeO_3)_2$. This is mainly attributed to their limited contribution to the anisotropy of polarizability. Consequently, there is an urgent need to develop a new method to achieve enhancement of the bandgap and birefringence in selenite materials.

Our research group has done many studies for the design and synthesis of selenite materials with a wide bandgap and large birefringence, and we have discovered that the bandgap of these materials can be influenced by the type of anionic group. Currently, we are pursuing two approaches to simultaneously improve the bandgap and birefringence of selenites. The first approach involves introducing SO_4 tetrahedral groups with a wide transmittance window,[31,32] exemplified by compounds like $Hg_2(SeO_3)(SO_4)$ (0.133 @ 532 nm, 3.58 eV)[33] and $Hg_3(SeO_3)_2(SO_4)$ (0.118 @ 546 nm, 4.70 eV).[34] Another approach involves the use of partially fluorinated metal oxide polyhedrons.[35,36] For instance, $CaYF(SeO_3)_2$ exhibits a wide bandgap of 5.06 eV and a large birefringence of 0.138 @ 532 nm.[37] It is noteworthy that there is still upside potential in enhancing the bandgap and birefringence of selenite compounds.

Based on our literature research, Si^{4+} in the IVA group exhibits a large bandgap and strong ultraviolet transmittance capability.[38,39] Additionally, F^- in the VIIA group has high electronegativity, strong ultraviolet transmittance capability, and chemical scissor action.[40–42] Combining these elements to form SiF_6 groups can leverage their individual advantages to positively influence the bandgap of compounds.[43,44] Moreover, SiF_6 groups can act as a chemical scissor, regulating the arrangement of metal cations and selenite ions, thereby enhancing the birefringence performance of the compounds. To achieve compounds with large birefringence, Pb^{2+} was chosen as the balancing cation. Aside from possessing stereo-chemically active lone pair electrons, Pb^{2+} readily forms highly anisotropic PbO_xF_y polyhedron when partially fluorinated.[45–47] The synergistic effect of the SiF_6 group, SeO_3 group, and PbO_xF_y polyhedron holds the potential for developing new selenite materials with a wide bandgap and large birefringence (Fig. 1). Consequently, we have focused our attention on the Pb^{2+}–Se^{4+}–Si^{4+}–F^-–O^{2-} system for the first time. As of now, no compounds have been discovered in this system. Through our exploration, a novel compound, $Pb_2(SeO_3)(SiF_6)$, has been obtained. $Pb_2(SeO_3)(SiF_6)$ stands as the initial example of a fluorosilicate selenite system. Theoretical calculations and experimental measurements indicate that the selenite fluorosilicate exhibits a large birefringence and a wide bandgap. The synergistic effect of the SeO_3 group, PbO_4 and PbO_3F_4 polyhedrons is the primary contributor to its large birefringence. This paper will report on the design, synthesis, structure, and optical properties of $Pb_2(SeO_3)(SiF_6)$.

Results and discussion

$Pb_2(SeO_3)(SiF_6)$ was synthesized using SeO_2, H_2SiF_6, and $Pb(BF_4)_2$ through a low-temperature (105 °C) hydrothermal method. The detailed synthesis procedures are outlined in the ESI† under the section titled "Syntheses". The elemental distribution map confirmed the presence of fluorine (F)
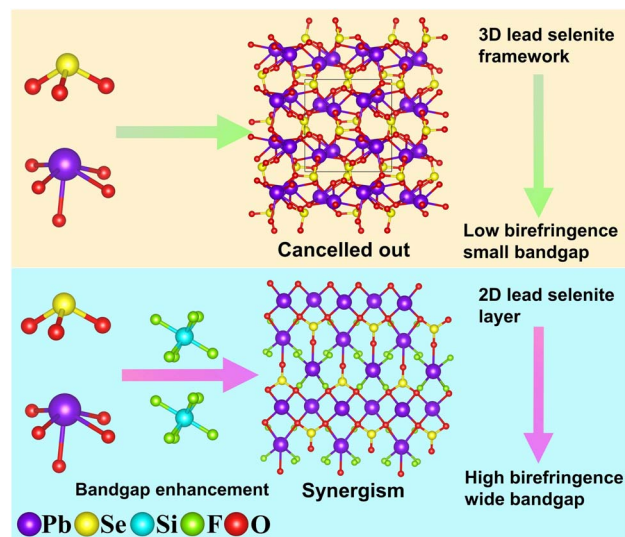

Fig. 1 From low birefringence, small bandgap to high birefringence wide bandgap regulated by SiF_6 groups.

element (Fig. 2), and quantitative elemental analysis results revealed the stoichiometry of F : Pb : Si : Se as 6 : 2 : 1 : 1 in the compound (Fig. S1a†). The crystal purity was verified using X-ray diffraction (XRD), as depicted in Fig. S1b.† Crystallographic details of $Pb_2(SeO_3)(SiF_6)$ can be found in Table S1.†

The first example of the selenite fluorosilicate compound, $Pb_2(SeO_3)(SiF_6)$, crystallizes in the orthorhombic space group *Pnma* (no. 62). The lattice parameters are $a = 13.8153(4)$ Å, $b = 5.4470(2)$ Å, $c = 9.6098(3)$ Å, $\alpha = \beta = \gamma = 90°$, and $V = 723.16(4)$ Å^3. Its asymmetric unit contains two lead atoms, one selenium atom, one silicon atom, four fluorine atoms, and two oxygen atoms, totaling ten atoms. Among them, F(1), F(4), and O(1) are located at general positions, while the remaining atoms occupy special positions. The selenium atom coordinates with three oxygen atoms, forming a trigonal pyramid with Se–O bond lengths ranging from 1.674(7) to 1.727(4) Å. The silicon atom bonds with six fluorine atoms, resulting in an octahedral SiF_6 configuration, with Si–F bond lengths ranging from 1.674(6) to 1.699(6) Å. Within the range of 2.5 to 2.8 Å, Pb(1) coordinates with four oxygen atoms, while Pb(2) coordinates with three oxygen and four fluorine atoms. Bond valence calculations indicate that the oxidation state of Se(1) is 3.958. The oxidation state of Si(1) is 4.513, which is relatively elevated and commonly observed in hexafluoro silicate compounds, such as compounds $KLiSiF_6$ (Si: 4.496),[48] Tl_2SiF_6 (Si: 4.506)[49] and Li_2SiF_6 (Si: 4.518).[50] Given that it is not an isolated case, we believe the high bond valence may be caused by the overestimated bond valence parameter (1.58) for the Si^{4+}–F bond. If the parameter was decreased to 1.55, the oxidation state of Si in $Pb_2(SeO_3)(SiF_6)$ will decrease to 4.16 and the same phenomenon is observed in $KLiSiF_6$ (Si: 4.15), Tl_2SiF_6 (Si: 4.15) and Li_2SiF_6 (Si: 4.16).[51] The calculated oxidation state for Pb(1) and Pb(2) is 1.374 and 1.443 respectively. The calculated oxidation state for Pb(1) and Pb(2) is 1.374 and 1.443 respectively. When considering the longer Pb–O and Pb–F bonds in the range of 2.80 to 2.97 Å, the
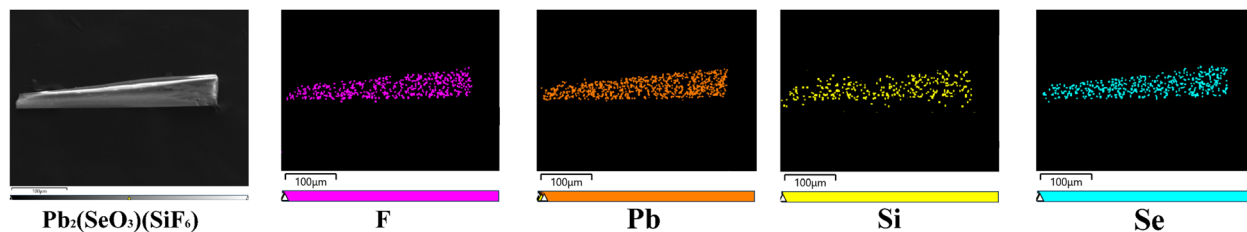
Fig. 2 SEM images of $Pb_2(SeO_3)(SiF_6)$ and its elemental distribution maps.

oxidation states of Pb(1) and Pb(2) can be increased to 1.868 and 1.755, respectively, approaching their standard oxidation states (Table S2†).

$Pb_2(SeO_3)(SiF_6)$ exhibits a novel three-dimensional (3D) structure composed of two-dimensional (2D) lead selenite layers bridged by SiF_6 groups (Fig. 3). Initially, several $Pb(1)O_4$ polyhedrons are linked through $O(1)\cdots O(1)$ edge-sharing, forming one-dimensional (1D) lead oxide chains. These chains are reinforced by $Pb(2)O_3F_4$ polyhedrons *via* O(1) atoms (Fig. 3a). The $Se(1)O_3$ groups serve as hexadentate ligands, coordinating bidentately with one Pb(1) atom and bridging to two Pb(1) and three Pb(2) atoms (Fig. 3b). These $Se(1)O_3$ groups further connect the 1D lead oxide chains to create a 2D lead selenite layer on the bc plane (Fig. 3d). Ultimately, the SiF_6 groups

bridge these 2D layers, resulting in the formation of a novel 3D $Pb_2(SeO_3)(SiF_6)$ network structure (Fig. 3e). Notably, the SiF_6 groups act as tridentate anionic ligands, coordinating bidentately with one Pb(2) atom and linking to two Pb(2) atoms (Fig. 3c). This complex configuration underscores the unique structural characteristics of the compound.

Thermogravimetric analysis (TGA) of the compound $Pb_2(SeO_3)(SiF_6)$ was performed within a temperature range of 20 to 1200 °C. It is noteworthy that the compound remains stable before reaching 220 °C. In the temperature range of 220 to 500 °C, the weight loss of the compound is primarily attributed to the decomposition of one molecule of SeO_2, with an experimental value of 15.8%, closely approximating the theoretical value of 16.2%. Beyond 500 °C, the weight loss of the compound should
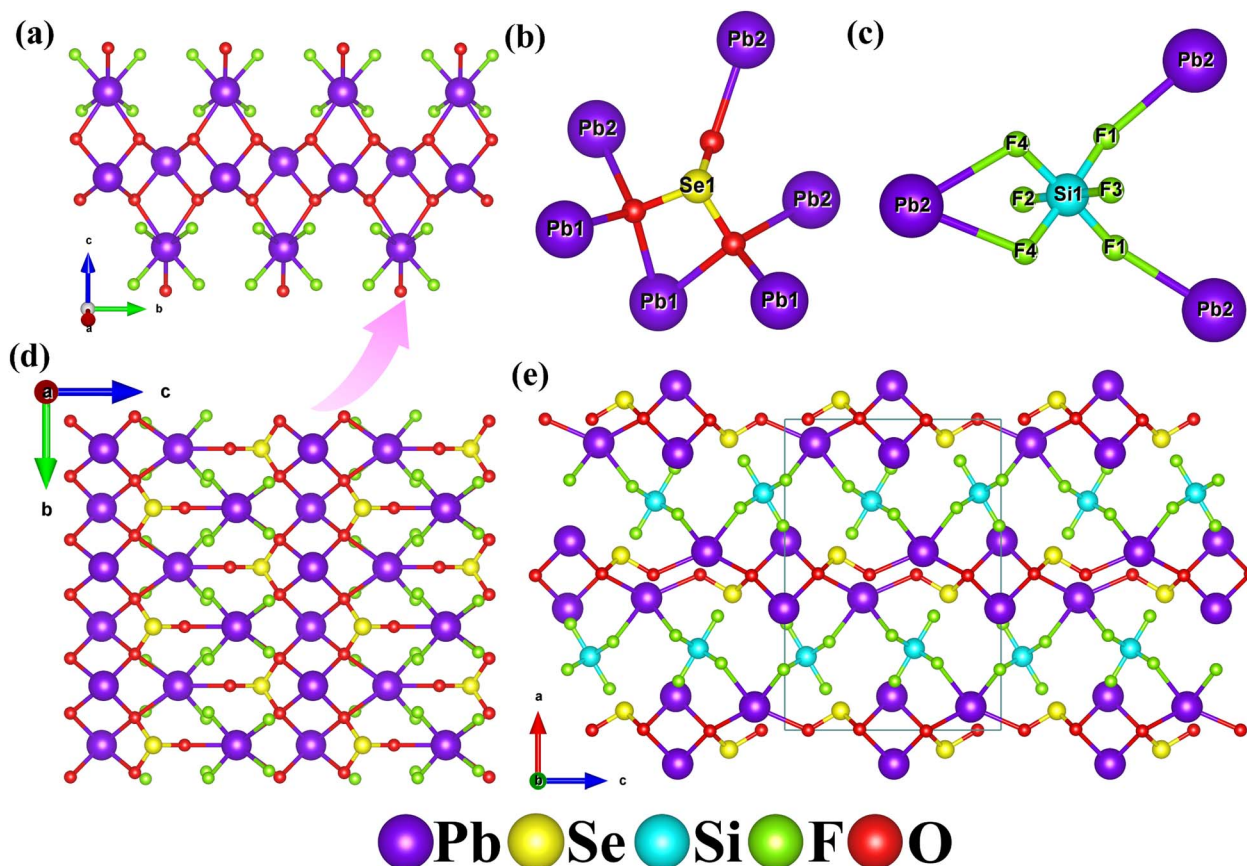

Fig. 3 One-dimensional lead oxide chains enhanced with lead oxyfluoride modification (a), the coordination environments of the SeO_3 group (b) and SiF_6 group (c), two-dimensional lead selenite layer structure (d) and the 3D structure of (e) $Pb_2(SeO_3)(SiF_6)$.

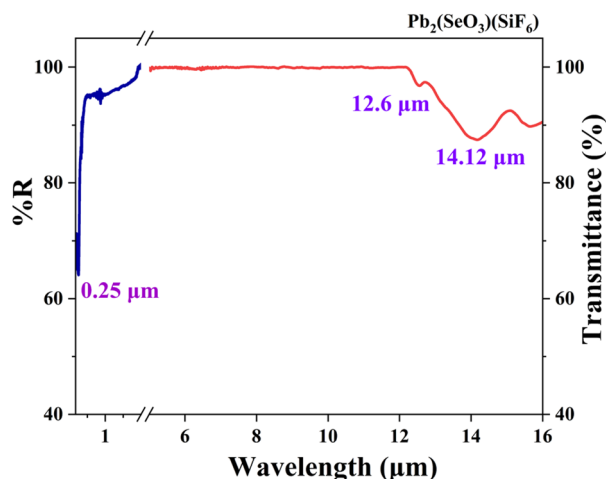**Fig. 4** UV-vis–NIR diffuse reflectance and IR transmittance spectra of $Pb_2(SeO_3)(SiF_6)$.

be associated with the incomplete decomposition of lead and fluorine components (Fig. S2†).[43] The incomplete weight loss of lead and fluorine components has been previously observed in the TGA of compounds $Pb_2Al_3F_3(Te_6F_2O_{16})$ and $Pb_2Ga_3F_3(Te_6-F_2O_{16})$, as reported by our group.[52] This further strengthens the reliability of our observations. In addition, $Pb_2(SeO_3)(SiF_6)$ also exhibits good environmental stability. The samples can still be stable after being exposed to room temperature for three months.

The infrared spectrum (IR) of $Pb_2(SeO_3)(SiF_6)$ was obtained at room temperature in the wavenumber range of 4000–400 cm^{-1}. The compound exhibits good transparency in the range of 4000–800 cm^{-1}. The characteristic peak observed around 638 cm^{-1} is attributed to the absorption of fluorine ions. Strong peaks in the regions of 420–510 cm^{-1} and 700–800 cm^{-1} are attributed to the bending and stretching vibrations of the Se–O bonds (Fig. S3†).

The UV-vis–NIR diffuse reflectance spectra indicate that the $Pb_2(SeO_3)(SiF_6)$ compound exhibits a UV cutoff edge at 247 nm, accompanied by a bandgap of 4.4 eV (Fig. S4†). Notably, this bandgap is significantly higher than those observed in previously reported lead-based compounds such as Pb_3SeO_5 (3.3 eV),[53] $CdPb_8(SeO_3)_4Br_{10}$ (3.32 eV),[45] $Pb_2Bi(SeO_3)_2Cl_3$ (3.45 eV),[20] $Pb_2NbO_2(SeO_3)_2Br$ (3.17 eV),[54] and $Pb_3(SeO_3)Br_4$ (3.35 eV).[55] This significant bandgap can be primarily attributed to the contribution of the perfluorinated group SiF_6. Combined with the IR spectrum, the transparency range for $Pb_2(SeO_3)(SiF_6)$ powder samples is from 0.25 to 12.6 μm (Fig. 4). However, considering the potential deviation in infrared cutoff edge due to multi-
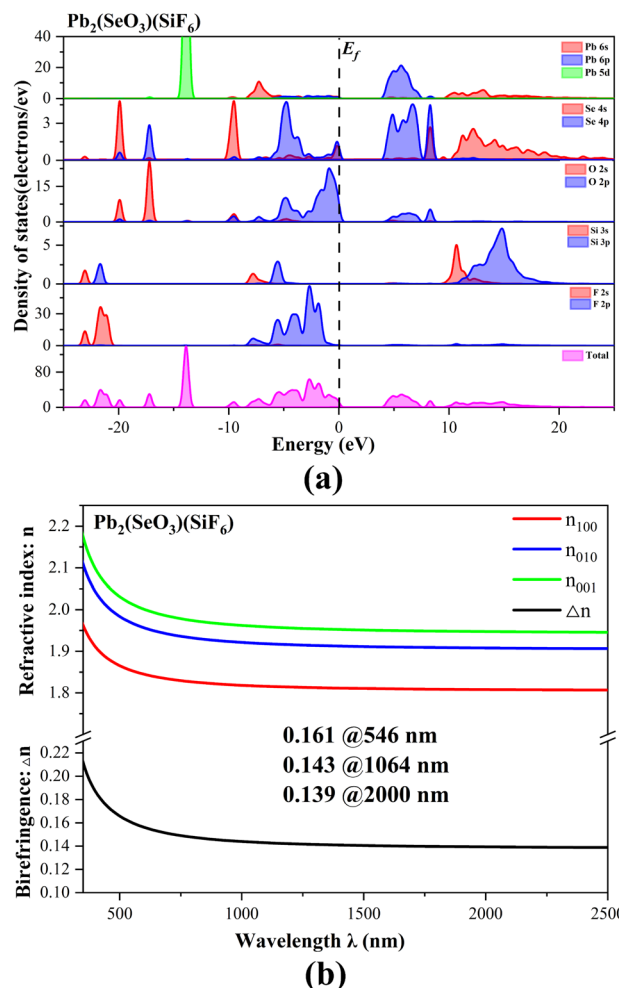

Fig. 6 The total and partial density of states (a) and the calculated refractive indices and birefringence values (b) of $Pb_2(SeO_3)(SiF_6)$.

phonon absorption in powder and crystal measurements, a 50% correction was applied.[56] Therefore, the estimated transparency range for $Pb_2(SeO_3)(SiF_6)$ should be from 0.25 μm to 6.3 μm, covering the ultraviolet, visible, and mid-infrared regions. This suggests that $Pb_2(SeO_3)(SiF_6)$ serves as a promising optical functional material.

A large bandgap is advantageous for enhancing the laser-induced damage threshold (LIDT) of compounds. Therefore, we measured the LIDT of $Pb_2(SeO_3)(SiF_6)$ within the particle size range of 150 to 210 nm. The experiments revealed that the LIDT
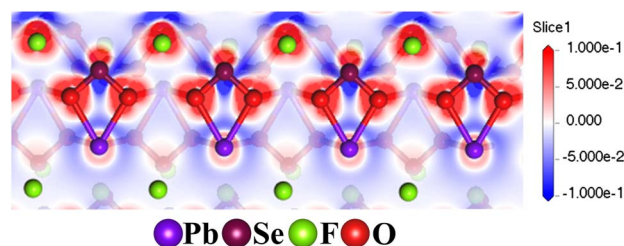

Fig. 5 Experimental birefringence at 546 nm for $Pb_2(SeO_3)(SiF_6)$.

Fig. 7 The electron density difference (EDD) map of $Pb_2(SeO_3)(SiF_6)$.

Table 1 The birefringence of reported selenite compounds with bandgap $\geq$4.2 eV

Compound	Space group	E_g (eV)	Birefringence	Ref.
$K_4(H_2SeO_3)(HSO_4)_2(SO_4)$	P-1	—	Cal.: 0.017 @ 1064 nm	59
$Pb_2Ga_3F_6(SeO_3)_2Cl_3 \cdot 2H_2O$	$R32$	4.59	Cal.: 0.02 @ 1064 nm	60
$NaGa_3(HSeO_3)_6(SeO_3)_2$	$P2_1/n$	5.2	Cal.: 0.03 @ 1064 nm	29
$Y_3F(SeO_3)_4$	$P6_3$	5.03	Cal.: 0.036 @ 1064 nm	37
$Ga_2(Se_2O_5)_2(HSeO_3)(H_2SeO_3)F$	$Pna2_1$	4.71	Cal.: 0.037 @ 1064 nm	61
$Na_8(SeO_3)(SO_4)_3$	$Pna2_1$	5.69	Cal.: 0.038 @ 1064 nm	59
$Y(HSeO_3)(SeO_3)(H_2O) \cdot (H_2O)$	$P2_12_12_1$	5.5	Cal.: 0.041 @ 1064 nm	30
$Cd_5Ga_4(HSeO_3)_2(SeO_3)_{10}$	P-1	4.7	Cal.: 0.044 @ 1064 nm	29
$Al(B(SeO_3)_3)H_2O$	$Pbca$	4.86	Cal.: 0.063 @ 1064 nm	62
$Ga(B(SeO_3)_3)H_2O$	$Pbca$	4.79	Cal.: 0.064 @ 1064 nm	62
$Ga_2(SeO_3)_3(H_2O)_3$	$R3c$	5.3	Cal.: 0.079 @ 1064 nm	29
$Ga(Se_2O_5)(HSeO_3)$	$P2_1/c$	4.34	Cal.: 0.079 @ 1064 nm	61
$Na_2(H_2SeO_3)(SO_4)$	$P2_1/c$	5.04	Cal.: 0.082 @ 1064 nm	59
$Al_2(SeO_3)_3(H_2O)_3$	$R3c$	5.5	Cal.: 0.084 @ 1064 nm	29
$Hf(SeO_3)_2$	$P2_1/c$	5.2	Cal.: 0.096 @ 1064 nm	63
$CsCl \cdot (H_2SeO_3)_2$	P-1	5.46	Cal.: 0.1 @ 532 nm	64
$Zr(SeO_3)_2$	$P2_1/c$	5.1	Cal.: 0.1025 @ 1064 nm	63
$Hg_3(SeO_3)_2(SO_4)$	$P2_1$	4.7	Cal.: 0.103 @ 1064 nm	34
$Sc(HSeO_3)_3$	Cc	5.28	Cal.: 0.105 @ 1064 nm	19
$Gd(NO_3)(Se_2O_5) \cdot 3H_2O$	$P2_12_12_1$	5.53	Cal.: 0.109 @ 1064 nm	65
$CaYF(SeO_3)_2$	$Pbcn$	5.06	Cal.: 0.127 @ 1064 nm	37
$NaLu(SeO_3)_2$	$Pna2_1$	5.3	Cal.: 0.128 @ 1064 nm	28
$CsCl\ H_2SeO_3$	$P2_1/c$	5.23	Cal.: 0.13 @ 532 nm	64
$RbCl \cdot (H_2SeO_3)_2$	P-1	5.39	Cal.: 0.14 @ 589 nm	66
$CsBr \cdot (H_2SeO_3)_2$	$P2_1/m$	5.19	Cal.: 0.14 @ 532 nm	64
$Pb_2(SeO_3)(SiF_6)$	**$Pnma$**	**4.4**	**Cal.: 0.161 @ 546 nm**	**This work**
$KCl \cdot (H_2SeO_3)_2$	P-1	5.44	Cal.: 0.17 @ 532 nm	64

value for $Pb_2(SeO_3)(SiF_6)$ is 50.8 MW cm^{-2}, approximately 19.5 times higher than that of $AgGaS_2$ (2.6 MW cm^{-2}). This value is slightly higher than those previously reported for the compounds $Hg_3Se(SeO_3)(SO_4)$ (23.35 MW cm^{-2})[57] and $Pb_3(TeO_3)Br_4$ (21.5 MW cm^{-2}).[45]

The birefringence of $Pb_2(SeO_3)(SiF_6)$ at 546 nm was measured using a Zeiss Axio Scope A1 polarizing microscope. Under positive polarization, $Pb_2(SeO_3)(SiF_6)$ exhibited complete extinction. The optical path difference was determined to be 1.365 μm, with a certain crystal plane at a thickness of 9.31 μm (Fig. S5†). Utilizing the formula $R = \Delta n \times T$,[58] the experimental birefringence of $Pb_2(SeO_3)(SiF_6)$ at 546 nm was determined to be 0.147 (Fig. 5). This result aligns with the theoretical birefringence value calculated in the subsequent text.

We have conducted an investigation into the electronic structure and optical properties of $Pb_2(SeO_3)(SiF_6)$ utilizing density functional theory.[67] The results show that $Pb_2(SeO_3)(SiF_6)$ is a direct bandgap compound, exhibiting a bandgap of 4.17 eV, which aligns closely with the experimental value of 4.4 eV (Fig. S6†). To ensure the precision of subsequent optical property calculations, we used a scissor operator of 0.23 eV. The partial and total density of states of $Pb_2(SeO_3)(SiF_6)$ are shown in Fig. 6a. Notably, the valence band top predominantly consists of O-2p and Se-4s4p orbitals, while the conduction band bottom is primarily composed of Se-4p and Pb-6p orbitals. This indicates that the bandgap of $Pb_2(SeO_3)(SiF_6)$ is mainly determined by Se, Pb, and O atoms.

To elucidate the theoretical birefringence of $Pb_2(SeO_3)(SiF_6)$, we calculated its birefringence using the formula $n^2(\omega) = \varepsilon(\omega)$.[68]

As a biaxial crystal, $Pb_2(SeO_3)(SiF_6)$ exhibits refractive index order: $n_{001} > n_{010} > n_{100}$. The theoretical birefringence values for $Pb_2(SeO_3)(SiF_6)$ are 0.161 at 546 nm, 0.143 at 1064 nm, and 0.139 at 2000 nm, showing a close agreement with the measured value of 0.147 at 546 nm (Fig. 6b). Fig. 7 illustrates the pronounced asymmetry of lobes on Se(IV), indicating of the high stereo–chemical activity of lone pairs, which is much larger than those of Pd(II). From the electron density difference (EDD) map, we can also find that the Se(IV) and Pb(II) groups are almost arranged in straight lines, which leads to the large birefringence of $Pb_2(SeO_3)(SiF_6)$. So, the large birefringence of $Pb_2(SeO_3)(SiF_6)$ was contributed by SeO_3, PbO_4 and PbO_3F_4 polyhedrons primarily. Although the SiF_6 groups contribute little to the birefringence of $Pb_2(SeO_3)(SiF_6)$ directly, the scissor effect of SiF_6 octahedrons make an important role in regulation of the arrangement of lone pair containing polyhedrons.

Table 1 provides a comprehensive summary of the birefringence of selenite compounds with bandgaps exceeding 4.2 eV reported to date.[18] It can be observed that $Pb_2(SeO_3)(SiF_6)$ exhibits a large birefringence in these selenites, second only to $KCl \cdot (H_2SeO_3)_2$ (0.17 @ 532 nm).[64] However, $Pb_2(SeO_3)(SiF_6)$ demonstrates the largest birefringence among the selenites without hydrogen, and it is the sole example of lead selenite with a large birefringence ($\Delta n \geq 0.1$) and wide bandgap ($E_g \geq 4.2$ eV). This result highlights the effectiveness of perfluorinated group modification in achieving dual enhancement of the bandgap and birefringence in selenite systems.

Conclusions

In summary, the first selenite fluorosilicate, $Pb_2(SeO_3)(SiF_6)$, has been successfully obtained through modification using per-fluorinated groups. The compound exhibits a unique 3D structure composed of 2D lead selenite layers interconnected by SiF_6 groups. Excitingly, $Pb_2(SeO_3)(SiF_6)$ achieves a balance between a wide bandgap and large birefringence. It represents a new birefringent crystal with large birefringence (0.161 @ 546 nm), a short UV cut-off edge (247 nm), a broad transmittance window (0.25–6.3 μm), a high laser-induced damage threshold (50.8 MW cm^{-2}) and excellent environmental stability. Notably, its birefringence is the largest among non-hydrogen selenite materials with bandgap ≥ 4.2 eV and stands as the only case of a lead selenite material with bandgap ≥4.2 eV and birefrin-gence ≥ 0.1. Theoretical calculations proved that the large birefringence of $Pb_2(SeO_3)(SiF_6)$ primarily originates from SeO_3 groups, PbO_4 and PbO_3F_4 polyhedrons. Our work not only pioneers a new selenite system, but also more importantly demonstrates the significance of perfluorinated groups modi-fication in the development of novel birefringent materials with a large bandgap.

Data availability

The data that support the findings of this study are available in the ESI† of this article.

Author contributions

Peng-Fei Li: investigation, formal analysis, and writing – orig-inal draft. Chun-Li Hu: theoretical calculations. Jiang-Gao Mao: supervision, resources, and funding acquisition. Fang Kong: conceptualization, project administration, and writing – review & editing. All authors have given approval to the final version of the manuscript.

Conflicts of interest

There are no conflicts to declare.

Acknowledgements

Notes and references

1 M. Mutailipu, J. Han, Z. Li, F. Li, J. Li, F. Zhang, X. Long, Z. Yang and S. Pan, *Nat. Photonics*, 2023, **17**, 694–701.

2 H. Y. Wu, C. L. Hu, M. B. Xu, Q. Q. Chen, N. Ma, X. Y. Huang, K. Du and J. Chen, *Chem. Sci.*, 2023, **14**, 9533–9542.

3 S. J. Han, A. Tudi, W. B. Zhang, X. L. Hou, Z. H. Yang and S. L. Pan, *Angew. Chem., Int. Ed.*, 2023, **62**, e202302025.

4 Z. Fang, W. H. Ma, Q. Y. Chen, X. T. Zhu, X. M. Zeng, P. B. Li, Q. F. Zhou, T. T. Song and M. H. Duan, *Inorg. Chem. Front.*, 2024, **11**, 1775–1780.

5 G. Zhou, J. Xu, X. Chen, H. Zhong, S. Wang, X. Ke, P. Deng and F. Gan, *J. Cryst. Growth*, 1998, **191**, 517–519.

6 G. Ghosh, *Opt. Commun.*, 1999, **163**, 95–102.

7 M. J. Cohen, H. Luo, E. L. Dereniak, T. Tkaczyk, R. Sampson and E. L. Dereniak, *presented in part at the Semiconductor Photodetectors III*, 2006.

8 M. J. Dodge, *Appl. Opt.*, 1984, **23**, 1980–1985.

9 J. R. DeVore, *J. Opt. Soc. Am.*, 1951, **41**, 416–419.

10 M. Cheng, W. Q. Jin, Z. H. Yang and S. L. Pan, *Chem. Sci.*, 2022, **13**, 13482–13488.

11 J. Guo, A. Tudi, S. Han, Z. Yang and S. Pan, *Angew. Chem., Int. Ed.*, 2021, **60**, 24901–24904.

12 Y. Lan, J. Ren, P. Zhang, X. Dong, L. Huang, L. Cao, D. Gao and G. Zou, *Chin. Chem. Lett.*, 2024, **35**, 108652.

13 M. Mutailipu, M. Zhang, Z. H. Yang and S. L. Pan, *Acc. Chem. Res.*, 2019, **52**, 791–801.

14 W. Zhou and S. P. Guo, *Acc. Chem. Res.*, 2024, **57**, 648–660.

15 H. Sha, D. Yang, Y. Shang, Z. Wang, R. Su, C. He, X. Yang and X. Long, *Chin. Chem. Lett.*, 2024, 109730.

16 M. Y. Ran, A. Y. Wang, W. B. Wei, X. T. Wu, H. Lin and Q. L. Zhu, *Coord. Chem. Rev.*, 2023, **481**, 215059.

17 J. Chen, C. Lin, X. Jiang, G. Yang, M. Luo, X. Zhao, B. X. Li, G. Peng, N. Ye, Z. Hu, J. Wang and Y. Wu, *Mater. Horiz.*, 2023, **10**, 2876–2882.

18 P. F. Li, J. G. Mao and F. Kong, *Mater. Today Phys.*, 2023, **37**, 101197.

19 Z. Bai, J. Lee, H. Kim, Y. Kuk, M. H. Choi, C. L. Hu and K. M. Ok, *Small*, 2023, **19**, 2207709.

20 Y. J. Jia, X. Y. Zhang, Y. G. Chen, X. X. Jiang, J. N. Song, Z. S. Lin and X. M. Zhang, *Inorg. Chem.*, 2022, **61**, 15368–15376.

21 S. S. Shi, C. S. Lin, G. S. Yang, L. L. Cao, B. X. Li, T. Yan, M. Luo and N. Ye, *Chem. Mater.*, 2020, **32**, 7958–7964.

22 Y. P. Gong, C. L. Hu, F. Kong and J. G. Mao, *Chem.–Eur. J.*, 2019, **25**, 3685–3694.

23 L. Lin, X. X. Jiang, C. Wu, Z. S. Lin, Z. P. Huang, M. G. Humphrey and C. Zhang, *Dalton Trans.*, 2021, **50**, 7238–7245.

24 Y. X. Ma, P. F. Li, C. L. Hu, J. G. Mao and F. Kong, *Adv. Sci.*, 2023, **10**, 2304463.

25 J. Ren, H. Cui, L. Cheng, Y. Zhou, X. Dong, D. Gao, L. Huang, L. Cao and N. Ye, *Inorg. Chem.*, 2023, **62**, 21173–21180.

26 Y. P. Gong, C. L. Hu, Y. X. Ma, J. G. Mao and F. Kong, *Inorg. Chem. Front.*, 2019, **6**, 3133–3139.

27 P. F. Li, C. L. Hu, F. Kong and J. G. Mao, *Inorg. Chem.*, 2023, **62**, 8494–8499.

28 P. F. Li, C. L. Hu, J. G. Mao and F. Kong, *Mater. Horiz.*, 2024, **11**, 1704–1709.

29 P. F. Li, Y. P. Gong, C. L. Hu, B. Zhang, J. G. Mao and F. Kong, *Adv. Opt. Mater.*, 2024, **12**, 2301426.

30 P. F. Li, C. L. Hu, B. X. Li, F. Kong and J. G. Mao, *J. Alloys Compd.*, 2023, **959**, 170570.

31 P. Zhang, X. Mao, X. Dong, L. Huang, L. Cao, D. Gao and G. Zou, *Chin. Chem. Lett.*, 2023, 109235, DOI: 10.1016/j.cclet.2023.

32 P. F. Li, C. L. Hu, Y. F. Li, J. G. Mao and F. Kong, *J. Am. Chem. Soc.*, 2024, **146**, 7868–7874.

33 P. F. Li, C. L. Hu, F. Kong and J. G. Mao, *Mater. Chem. Front.*, 2022, **6**, 3567–3576.

34 J. Ren, Y. Chen, L. Ren, Y. Zhou, X. Dong, D. Gao, L. Huang, L. Cao and N. Ye, *Inorg. Chem.*, 2023, **62**, 9130–9138.

35 H. Qiu, S. Pan and M. Mutailipu, *Fundam. Res.*, 2023, DOI: 10.1016/j.fmre.2023.08.017.

36 C. Shen, F. Zhang, T. Sasaki, C. Eerdun, M. Hayashi, H.-w. Wang, K. Tominaga, M. Mutailipu and S. Pan, *Angew. Chem., Int. Ed.*, 2024, **63**, e202319121.

37 P. F. Li, C. L. Hu, F. Kong and J. G. Mao, *Angew. Chem., Int. Ed.*, 2023, **62**, e202301420.

38 Y. Yang, Y. Xiao, B. Li, Y. G. Chen, P. Guo, B. Zhang and X. M. Zhang, *J. Am. Chem. Soc.*, 2023, **145**, 22577–22583.

39 G. Xu, H. Li, J. Han, X. Hou, Z. Yang and S. Pan, *Inorg. Chem.*, 2023, **63**, 852–859.

40 H. Qiu, F. Li, C. Jin, Z. Yang, J. Li, S. Pan and M. Mutailipu, *Angew. Chem., Int. Ed.*, 2023, **63**, e202316194.

41 Y. Hu, X. Jiang, T. Wu, Y. Xue, C. Wu, Z. Huang, Z. Lin, J. Xu, M. G. Humphrey and C. Zhang, *Chem. Sci.*, 2022, **13**, 10260–10266.

42 M. Yan, R. L. Tang, W. D. Yao, W. Liu and S. P. Guo, *Chem. Sci.*, 2024, **15**, 2883–2888.

43 R. L. Tang, X. Lian, W. D. Yao, W. Liu and S. P. Guo, *Dalton Trans.*, 2021, **50**, 16562–16567.

44 Y. Shen, Y. Zhou, X. Xue, H. Yu, S. Zhao and J. Luo, *Inorg. Chem. Front.*, 2022, **9**, 5226–5230.

45 P. F. Li, C. L. Hu, B. X. Li, J. G. Mao and F. Kong, *Inorg. Chem. Front.*, 2023, **10**, 7343–7350.

46 C. Bai, Y. Chu, J. Zhou, L. Wang, L. Luo, S. Pan and J. Li, *Inorg. Chem. Front.*, 2022, **9**, 1023–1030.

47 Y. Y. Yang, Y. Guo, B. B. Zhang, T. Wang, Y. G. Chen, X. H. Hao, X. X. Yu and X. M. Zhang, *Inorg. Chem.*, 2022, **61**, 1538–1545.

48 C. Stoll, M. Seibald, D. Baumann, J. Bandemehr, F. Kraus and H. Huppertz, *Eur. J. Inorg. Chem.*, 2021, **2021**, 62–70.

49 J. Rienmüller, J. Bandemehr and F. Kraus, *Z. Naturforsch., B: J. Chem. Sci.*, 2021, **76**, 559–565.

50 W. Hinteregger, H. Niederwieser and Z. Huppertz, *Kristallogr*, 2014, **229**, 77–82.

51 B. N. E. Brese and M. O'Keeffe, *Acta Crystallogr.*, 1991, **B47**, 192–197.

52 P. F. Li, F. Kong and J. G. Mao, *J. Solid State Chem.*, 2020, **286**, 121288.

53 S. H. Kim, J. Yeon and P. S. Halasyamani, *Chem. Mater.*, 2009, **21**, 5335–5342.

54 H. Zhao, P. Gong, X. Zhang, Z. Lin, Z. Hu and Y. Wu, *Dalton Trans.*, 2020, **49**, 14046–14051.

55 X. X. Wang, X. X. Jiang, H. M. Liu, L. Yang, Z. S. Lin, Z. G. Hu, X. G. Meng, X. G. Chen and J. G. Qin, *Dalton Trans.*, 2018, **47**, 1911–1917.

56 Z. Yang, C. Hu, M. Mutailipu, Y. Sun, K. Wu, M. Zhang and S. Pan, *J. Mater. Chem. C*, 2018, **6**, 2435–2442.

57 P. F. Li, C. L. Hu, B. X. Li, J. G. Mao and F. Kong, *Inorg. Chem.*, 2024, **63**, 4011–4016.

58 H. Y. Sha, Y. R. Shang, Z. J. Wang, R. B. Su, C. He, X. M. Yang and X. F. Long, *Small*, 2023, e2309776, DOI: 10.1002/smll.202309776.

59 X. W. Zhang, Z. X. Wang, C. L. Hu, Y. F. Li, J. G. Mao and F. Kong, *Inorg. Chem.*, 2024, **63**, 6067–6074.

60 L. Liu, J. Wang, B. Xiao, X. Li, Y. Chu, T. Sun and P. S. Halasyamani, *J. Mater. Chem. C*, 2024, **12**, 4986–4994.

61 J. Zhang, H. Yu, Z. Hu, J. Wang, Y. Wu and H. Wu, *Mater. Today Phys.*, 2023, **35**, 101145.

62 M. Y. Cao, C. L. Hu, F. Kong, Z. Y. Xiong and J. G. Mao, *Dalton Trans.*, 2021, **50**, 15057–15061.

63 J. Lv, Q. Li, X. Guan, N. Lin, J. Zhang, Z. Jia and X. Tao, *CrystEngComm*, 2023, **25**, 1675–1682.

64 M. Zhu, J. Wang, L. Hou, Y. Yuan, L. Liu, Y. Chu and C. Huang, *Inorg. Chem.*, 2024, **63**, 2289–2297.

65 C. Wu, L. H. Li, L. Lin, Z. P. Huang, M. G. Humphrey and C. Zhang, *Dalton Trans.*, 2020, **49**, 3253–3259.

66 H. Wang, L. Liu, Z. Hu, J. Wang, M. Zhu, Y. Meng and J. Xu, *Inorg. Chem.*, 2022, **62**, 557–564.

67 C. L. Hu, Y. X. Han, Z. Fang and J. G. Mao, *Chem. Mater.*, 2023, **35**, 2647–2654.

68 H. Chen, M. Y. Ran, S. H. Zhou, X. T. Wu, H. Lin and Q. L. Zhu, *Chin. Chem. Lett.*, 2023, **34**, 107838.